Design of a Pneumatic Muscle Based Continuum Robot with Embedded Tendons

Rongjie Kang*, Yong Guo, Lisha Chen, David T. Branson, Jian S. Dai

***Abstract* — Continuum robots have attracted increasing focus in recent years due to their intrinsic compliance that allows for dexterous and safe movements. However, the inherent compliance in such systems reduces the structural stiffness, and therefore leads to the issue of reduced positioning accuracy. This paper presents the design of a continuum robot employing tendon embedded pneumatic muscles (TEPMs). The pneumatic muscles are used to achieve large scale movements for preliminary positioning while the tendons are used for fine adjustment of position. Such hybrid actuation offers the potential to improve the accuracy of the robotic system, while maintaining large displacement capabilities. A 3-dimensional (3-D) dynamic model of the robot is presented using a mass-damper-spring based network, in which elastic deformation, actuating forces and external forces are taken into account. The design and dynamic model of the robot are then validated experimentally with the help of an electromagnetic tracking system.**

***Index Terms* — Continuum robots, Pneumatic muscles, Embedded tendons, Hybrid actuation**

I. Introduction

Conventional robots employing rigid links connected by actuated joints have been used extensively in industry where high stiffness and fast dynamics are required. However, their motions are significantly constrained by the limited number of degrees-of-freedom (DOF) and minimal deformation at the joints and links. In recent years increasing demand for highly dexterous and human-friendly manipulation has encouraged the developments of continuum robots inspired by soft organs in nature such as the elephant trunk, octopus tentacle, etc. Such robots are constructed with soft or semi-soft materials, and therefore have a continuously deformable body and large number of DOF. This means that they are able to adapt to unstructured environments to perform tasks such as search and rescue in narrow workspaces, minimally invasive surgery, etc.

There have been numerous attempts to design and implement continuum robots. Walker et al. [1,2] developed a series of continuum robots to mimic the morphology and motions of an elephant trunk, most of which were driven by pneumatic muscles. Yuk et al. [3] and Menciassi et al. [4] designed worm-like crawling robots actuated by Shape Memory Alloy (SMA). Choi et al. [5] presented a hyper-redundant robotic arm equipped with Electro-Active Polymer (EAP) based actuators. Camarillo et al. [6] developed a tendon-driven continuum manipulator for use in a cardiac catheter. Laschi et al. [7] built an octopus-inspired soft robot employing steel cables that is capable of manipulation and locomotion. Althoefer et al. [8] utilized double-layer planar springs and tendons to construct a continuum manipulator. Dai et al. [9] presented a continuum robot with integrated origami structures. By reviewing the previous designs, it is found that the intrinsically compliant actuators used in continuum robots can be classified into the following actuation categories: pneumatic muscles, tendon-driven mechanisms, Electro-Active Polymers (EAP), and Shape Memory Alloys (SMA).

One of the prime motivations of implementing the above actuators are due to their compliant body that can deform passively to adapt to unstructured environments, reducing the complexity of active control. However, to achieve desired locomotion and manipulation against external force disturbances, performances such as stiffness, accuracy and dynamics need to be appropriately blended with compliance in the actuator design for continuum robots. Pneumatic muscles are capable of producing large scale movements with high speeds and strength, but introduce nonlinearities, such as dead zone and hysteresis, to the system, and therefore reduce control accuracy [10]. Tendon-driven mechanisms are more accurate, but they are not able to actively resist compressive loads. SMA and EAP based actuators are easier and more efficient for control as they convert electrical energy to movements directly. However, their application is limited by the relatively low speeds and/or small output forces [11], and the SMA actuation suffers from strong hysteresis and the generation of significant heat. So far none of the above actuation approaches can provide continuum robots with a comprehensive performance to achieve accuracy, strength, and good dynamic performance at the same time.

To improve the performance of continuum robots, methods to combine multiple actuation technologies were proposed. Immega et al. [12] and Walker et al. [13] developed the KSI

Manuscript received XX-XX-2016. This work was supported by the Natural Science Foundation of China (Grant No. 51375329, No.51605329 and No. 51611130202), Tianjin Municipal Science and Technology Department Program (Grant No.13JCZDJC26400), and the International S&T Cooperation Program of China (Grant No. 2014DFA70710).

Rongjie Kang and Yong Guo are with the Key Laboratory of Mechanism Theory and Equipment Design of Ministry of Education, School of Mechanical Engineering, Tianjin University, Tianjin China. (e-mail: rjkang@tju.edu.cn, guoyong@tju.edu.cn)

Lisha Chen is with the School of Mechanical Engineering, Tianjin Polytechnic University, Tianjin, China. (e-mail: lisha.chen@foxmail.com)

David T. Branson is with the Faculty of Engineering, University of Nottingham, UK. (e-mail: david.branson@nottingham.ac.uk)

Jian S. Dai is with the Centre for Robotics Research, School of Physical Sciences and Engineering, King's College, London, UK. (e-mail: jian.dai@kcl.ac.uk)

tentacle manipulator and Air-Octor robot, respectively. These robots utilized a similar design composed of a pneumatically-pressurized central chamber and surrounding tendons. The central chamber was used to provide the structural support and to control the extension/contraction along the backbone axis, while the tendons used to control bending motions. This meant that the full benefits of hybrid actuation are not achieved as the actuation elements are utilized separately, instead of working in tandem. Laschi et al. [14] presented a tendon+SMA hybrid actuation mechanism for an octopus-like continuum robot, exhibiting highly flexible motions. However, neither the tendon nor the SMA can take compression, so a silicone tube was used to contain the actuators and form the body structure. The output strength of this robot was therefore relatively low in comparison with those using pneumatic muscle actuation. Other hybrid actuation methods focused on improving stiffness and accuracy of compliant continuum robots. Shiva et.al. [15] designed a pneumatically actuated soft manipulator whose stiffness can be further adjusted by tendons. Ciancetti et al. [16] integrated a jamming mechanism to a pneumatic soft robot to adjust its stiffness. Conrad and Zinn [17] presented an interleaved continuum-rigid manipulator which combines flexible actuated segments with more precise embedded rigid-link joints. Although hybrid actuation may increase the weight and size of a robotic system, it is applicable to those applications where relatively stiff and accurate control of a continuum robot is required, e.g. holding the end-effector at a specific position to perform tasks.

Another challenge in developing continuum robots comes in the development of accurate and robust models for such inherently compliant structures. The kinematics of such robots have been extensively investigated [1, 18-20]. However, to consider the influence of actuating forces, external forces and structural deformation, dynamic information needs to be further included in the model. Tatlicioglu et al. [21] used the work-energy principle and Lagrangian formulation to obtain the dynamic model for a planar continuum robot. Later they extended this method to consider the potential energy including the gravitational and elastic potential energy [22]. Jones et al. [23] used the Cosserat rod theory to analyze the 3-D statics for continuum robots. Giri et al. [24] and Yekutieli et al. [25] used the mass-spring system to model octopus-tentacle-like robots in 2-D space. Qiu et al. [26] presented a repelling-screw based approach to model the reaction force of origami-inspired continuum robots when they are deformed. Kang et al. [27] utilized a number of serially connected parallel mechanisms to represent the continuum robot so that the movements can be analyzed by using the theory of rigid body dynamics. However, these methods are still limited in that the work-energy principle is based on the assumption of constant curvature [21, 22], which is sometimes not accurate, and might pose a problem when using such models for precise control of continuum robots. Dynamic models using the Cosserat rod theory only considered static solutions, moreover, they simplified the robot to a planar or spatial curve where external loads or actuating forces cannot be accounted for appropriately [23]. The mass-spring system used in [24] and [25] can reflect the dynamic behaviors of soft bodies but was limited to the planar cases. The 3-D model reported in [27] is still within the scope of rigid body dynamics, and therefore has difficulties in describing elastic deformation.

The aim of this paper is to find a possible solution to achieve design balance among dexterity, accuracy and strength for continuum robots. A key point to this is the development of a new actuation system enabling large scale movements and high strength with the capability to achieve higher accuracy. As mentioned above, the pneumatic muscles are able to achieve large scale movements and high strength, but lack accuracy. While the tendon-driven mechanisms possess high movement resolution, and are therefore suitable for small scale movements at high accuracy. This work combines the advantages of both pneumatic muscles and tendon-driven mechanisms to construct a novel, hybrid actuator for continuum robots where the pneumatic muscles are used to provide structural support and coarse positioning, while the tendons used to provide fine positioning. A dynamic model of the continuum robot equipped with the hybrid actuators is then presented based on a mass-damper-spring network that is able to predict the motions and elastic deformation of the robot with respect to actuation and external forces.

The paper is organized as follows: in Section 2 the mechanical design of the robot and its actuators is presented; in Section 3 the dynamic model is defined and identified; Section 4 provides the experimental results and conclusions are given in Section 5.

II. Prototype Design

In this section, the design of a novel continuum robot partially inspired by the anatomy of an octopus arm and additionally equipped with hybrid actuation is presented.

A. Bio-inspired Robotic Structure

A paradigmatic example in nature of continuum structure is the octopus arm. It is able to elongate/shorten along its length and bend in any direction, and to grasp irregularly shaped objects. This particular dexterity is due to its boneless structure and muscular arrangement which is composed of three types of muscles: the longitudinal, radial and oblique muscles [2,14,28]. It has been found that the longitudinal and radial muscles are divided into four groups and arranged in parallel, while the oblique muscles cover the arm diagonally, Fig.1 (a), [25]. As these biological muscles are only able to contract, the longitudinal and radial muscles need to work antagonistically to control the arm to elongate, shorten and bend. Contraction of the oblique muscles is what results in twist motion [2, 25].

From a kinematic viewpoint, the use of four groups of longitudinal/radial muscles is redundant. In engineering applications the muscular structure of an octopus arm can be simplified to a 3-DOF parallel mechanism as shown in Fig.1(b), [2, 26]. To illustrate the motion of a single module, a local coordinate system *O-uvw* is attached to the bottom of the module, where the origin *O* is at the centroid of the bottom plane, the axis *u* is along the central axis of the module and the axis *w* passing through the bottom end of the actuator A_3. Three

This article has been accepted for publication in a future issue of this journal, but has not been fully edited. Content may change prior to final publication. Citation information: DOI 10.1109/TMECH.2016.2636199, IEEE/ASME Transactions on Mechatronics

longitudinal actuators, A_1, A_2 and A_3, in this system composed of Tendon Embedded Pneumatic Muscles (TEPMs) further discussed in Section 2.2, are capable of actively changing their length to achieve 1-DOF elongation/contraction along the central axis *u*, and 2-DOF bending motion about the axes *w* and *v* due to the parallel arrangement of the actuators. The twist motion about axis *u* is not considered at this stage but could be achieved by mounting the robot on a rotary base platform in the future. To form a continuum robot, a number of robotic modules consisting of such 3-DOF parallel mechanism can then be stacked serially. The use of more modules will increase the total DOF of the robotic system, i.e. an increase of the dexterity, but it will also increase the load to the proximal modules. Form this viewpoint, the proximal modules should be designed more stiff than the distal modules. Considering that this work focuses on the development a hybrid actuation method rather than the structural analysis for a continuum robot, a prototype with two identical modules is then enough for demonstration, in which the proximal module is capable of taking the load from the distal module.

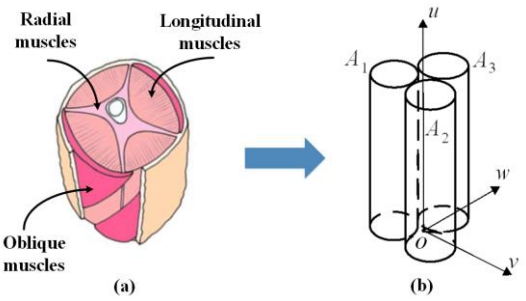

Fig. 1. A 3-DOF parallel mechanism inspired by octopus arm anatomy

The robotic prototype presented in this paper, Fig. 2(a), is 430mm in length and constructed using two identical modules. The TEPM actuators in module 1 are denoted as $A_{1,1}$, $A_{1,2}$ and $A_{1,3}$, while the ones in module 2 denoted as $A_{2,1}$, $A_{2,2}$ and $A_{2,3}$. Thus each module is capable of 3-DOF motion and the robotic system achieves 6 DOFs in total. The robot employs a hybrid actuation system including pneumatic and tendon-driven units, as shown in Fig.2(b). The pressure can be tuned by the pneumatic regulators to control the length of each TEPM for large scale movements. In addition, a motor-pulley system is used to apply tension through a tendon to the TEPM for fine adjustment of its length.

The control hardware of the robot is presented in Fig.2(c). A host computer is used for generating the control commands, e.g. muscle pressure and tendon tension, and sending these commands to an Arduino based control board through an RS-232 serial link. The Arduino board converts the control commands to analog voltages and impulse signals that are used as inputs to the pneumatic regulators and stepping motor drivers respectively to change the length of the TEPMs and therefore the position of the robot. A 3-D electromagnetic tracking system (Ascension, produced by NDI), is used to feedback the position of the TEPMs and robot to the host computer. 4 sensors, s_i (i=1,2,3,4), are mounted in the plastic holders along the robot length from the base to the tip, Fig.2(a), and tracked by the 3-D electromagnetic system in real time. The root mean square error for position tracking is below 1.0mm.

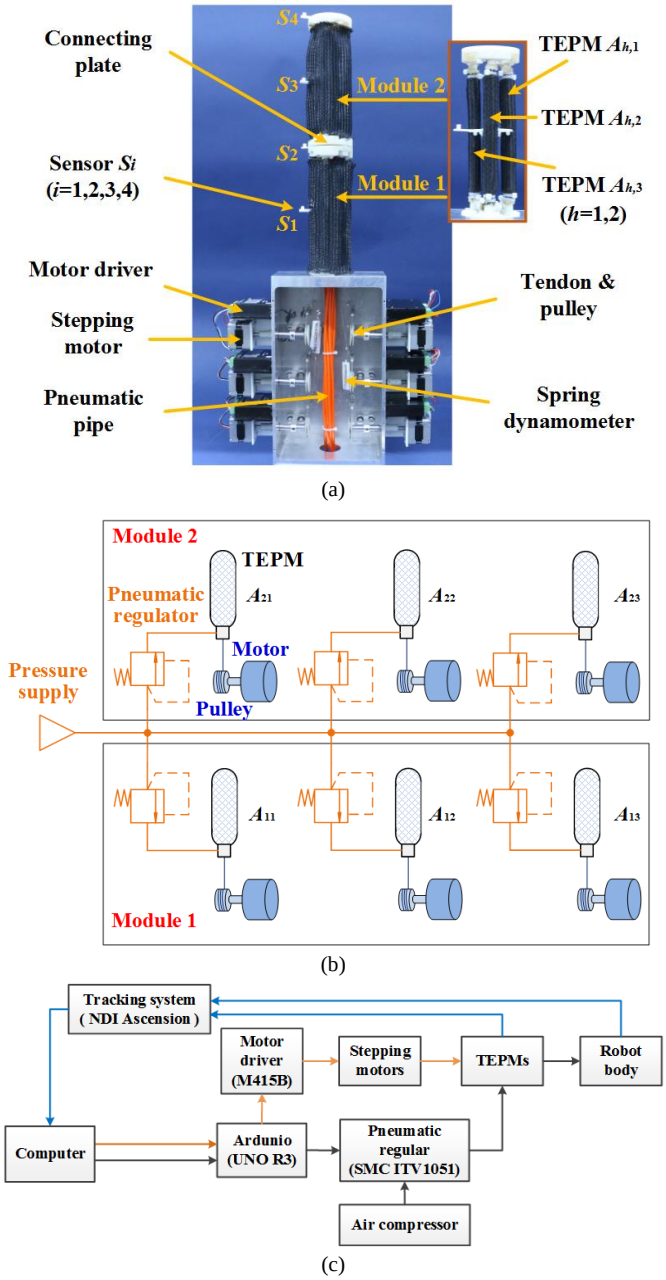

Fig. 2. The robotic prototype (a) overview (b) schematic of the mechanical system (c) configuration of the control hardware

B. Tendon Embedded Pneumatic Muscle (TEPM)

As mentioned above, the TEPM actuator has a hybrid structure combining a pneumatic muscle with an embedded tendon, each of which are controlled independently. The pneumatic pressure is provided by an air compressor and tuned individually using pneumatic regulators (SMC ITV1051) for each muscle. The pneumatic muscle is composed of an outer nylon braided sheath, inner silicone tube and helical spring as shown in Fig.3. The nylon sheath and silicone tube are mounted to an end-cap at one end and to a pneumatic connector at the other end. As the sheath is initially compressed giving a mesh angle greater than 54.7 degrees, the muscle will elongate when

inflated [29].The spring is implanted into the wall of the silicone tube to prevent the silicone tube from expanding radially, and provides a resilient force so that the pneumatic muscle can return to straight position when deflated. In comparison with previous pneumatic muscles using pure silicone or rubber materials [27,30], the integration of a resilient spring makes the muscle stiffer and more controllable, especially when undergoing lateral forces perpendicular to the longitudinal axis of the muscle.

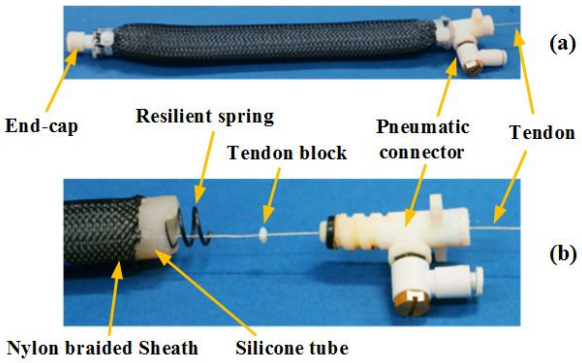

Fig. 3. TEPM Configuration (a) Overview of a TEPM (b) Exploded view of the TEPM

From the previous design reported in [30] it was found that the positioning accuracy of pneumatic muscles were greatly reduced when bundled together in parallel to form the body structure of a continuum robot. This is because the friction and interaction forces between individual muscles will bring unpredictable non-linearities such as hysteresis and dead-zone operation points to the pneumatic muscles. To solve this problem, an additional tendon made of a steel cable is arranged inside of the pneumatic muscle. This tendon is fixed to the end-cap at one end of the pneumatic muscle and passes through the pneumatic connector at the other end. A rubber gasket is placed in the pneumatic connector to prevent air leaking. The tendon blocks, one of which is shown in Fig.3(b), will slide along with the tendon in the silicone tube and maintain the space between the tendon and the inner surface of the silicone tube. In this way, the tendon is approximately coaxial with the pneumatic muscle during bending movements. In the prototype the tendon is driven by a stepping motor and a spring dynamometer is utilized to measure the applied tension. The TEPM actuator will contract if the motor attached to the tendon cable pulls on it through a pulley system. In this way, the actuator can achieve small length changes in addition to large scale movements achieved with the pneumatic muscles. The axial length of a single TEPM is therefore given by

$$L = L_0 + \Delta L_p + \Delta L_t + \Delta L_e = L_0 + \frac{pA}{K_a} - \frac{\tau / R}{K_a} + \frac{F_e}{K_a} \qquad (1)$$

where L_0 is the initial length of the actuator that is a constant , ΔL_p is the length change caused by the pneumatic pressure p , ΔL_t is the length change caused by the tendon tension that is proportional to the motor torque τ , ΔL_e is the length change caused by the axial external force F_e, A is the cross-section area of the silicone tube, R is the radius of the pulley, and K_a is the equivalent stiffness of the TEPM identified in Section 3. Note that, a positive change in pressure will cause a positive change in actuator length while a positive change in tension will cause a negative change in actuator length, thus, a minus "-" is used in front of the tension, τ / R , in (1). The pneumatic pressure drives the TEPM to an approximate length while the tendon tension is used to finely adjust the final length. As the tendons are embedded in the pneumatic muscles the size of the muscle does not increase. Parameters of the TEPM and robotic prototype are given in table I.

Table I Parameters of the robotic prototype

Parameter	Description	Value	Unit
L_o	Initial length of the TEPM	200	mm
A	Cross-section area of the silicone tube	50.27	mm^2
R	Radius of the pulley	15	mm
m_d	Mass of a module	0.22	kg
m_t	Mass of a TEPM	0.05	kg
K_s	Stiffness of the resilient spring	290	N/m

III. Modeling and Identification

A mass-damper-spring network is used to model the presented compliant continuum robot in which the effects of actuation forces, external forces, and structural deformation are considered. The presented modeling method is generic and can be adapted to a wide range of continuum robots with soft or semi-soft structures.

A. Dynamic Model of the Robot

Composed of three longitudinal actuators, one module of the continuum robot can be considered as a triangle prism in the workspace [30]. The prism is divided into n segments to obtain a distributed parameter model, where accuracy and computational time depend on the number of segments in the model. The use of more segments will provide higher model accuracy but increase the computational time and vice versa. In previous work, each segment was equivalent to a rigid parallel mechanism [27], however, the robotic module in question is actually an elastic mechanism rather than a rigid one. This paper therefore utilizes a mass-damper-spring network based dynamic model, enabling intrinsic compliance to be considered.

Two segments are chosen as an example for illustration, Fig. 4. Each node of the segments is considered as a mass point connected to its adjacent nodes with a damper and spring to form a mass-damper-spring system. Considering the adjacent nodes along the vertical edge are also connected by the longitudinal actuators, a D-S-A unit composed of a damper, spring and actuator is used to represent the vertical edge while a D-S unit composed of a damper and a spring is used to connect other adjacent nodes along the horizontal edges and in the diagonal directions.

This article has been accepted for publication in a future issue of this journal, but has not been fully edited. Content may change prior to final publication. Citation information: DOI 10.1109/TMECH.2016.2636199, IEEE/ASME Transactions on Mechatronics

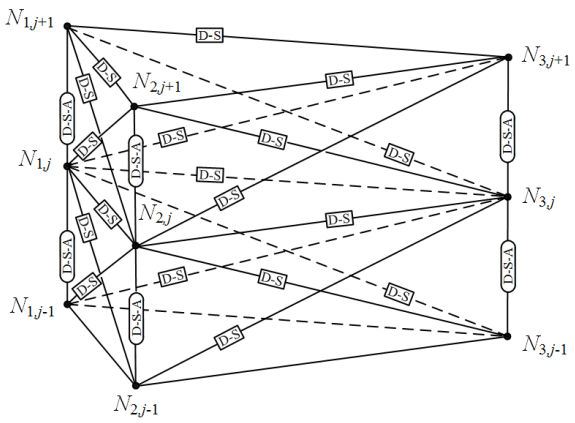

Fig. 4. Two segments represented by the mass-damper-spring systems (N_{ij}, $i=1,2,3$, $j=1,...n$-1)

Unlike previous distributed parameter models [27, 31], only one global coordinate system is required in this model to describe the movements of the mass points. The detailed formulation of the model can be found in [30]. The model is numerically solved using the fourth-order Runge-Kutta algorithm to obtain position, velocity and acceleration of all mass points.

B. Parameter Identification

There are three kinds of parameters that need to be identified in the dynamic model: the mass of the points, the damping coefficient and the spring constant. As the robot is divided into n segments and each of the two modules is composed of n_e segments, thus n=2n_e. Considering there are three actuators in one module, the number of the mass points in one module is 3n_e, and the mass of each point is then obtained by

$$m_{ij} = \frac{m_d}{3n_e} \tag{2}$$

where m_d is the total mass of the module. In this paper, n_e = 6 is used to achieve a trade-off between modeling accuracy and computational time cost.

From (1), the axial length change for a TEPM is

$$\Delta L=\Delta L_p+\Delta L_t+\Delta L_e=\frac{1}{K_a}(pA-\frac{\tau}{R})+\frac{F_e}{K_a}=\frac{F_a}{K_a}+\frac{F_e}{K_a} \tag{3}$$

where F_a is the total actuating force generated by both pneumatic muscle and tendon, F_e is the external force, and K_a is the equivalent stiffness of the TEPM which is along the vertical edge of the model shown in Fig.4. Previous works have indicated that the relationship between the input forces and the output length change of a pneumatic muscle is approximately linear [32,33], thus the TEPM actuator is considered as a spring system in this paper as well. To identify the equivalent stiffness K_a, it is not necessary to apply all the possible forces (pressure, tension, external loads) shown in (3) to a TEPM actuator simultaneously. In this paper, the value of K_a=358.86N/m is identified by the relationship between the input pressure p (from 0 to 0.5 MPa) and the corresponding length change ΔL_p (from 0 to 70mm) while the tension and external force are set to zero. It was found that the TEPM exhibits an approximately linear property while the pressure varies from 0.05MPa to 0.45 MPa.

Similarly, the value of damping coefficient along the vertical direction c_v=15.50Ns/m is obtained using the identification method reported in [27,30]. In this model, the stiffness and damping coefficients in the horizontal and diagonal directions are expressed by

$$\begin{cases} k_h = \alpha_1 k_v \\ k_d = \alpha_2 k_v \end{cases} \text{and} \begin{cases} c_h = \beta_1 c_v \\ c_d = \beta_2 c_v \end{cases} \tag{4}$$

where k_v = $n_e K_a$, α_1 and α_2 are the stiffness gains for the horizontal and diagonal springs respectively, β_1 and β_2 are the stiffness gains for the horizontal and diagonal dampers respectively. In this paper, α_1=70, α_2=1, and β_1 =β_2=1 are identified by minimizing the gap between the model and the prototype according to the method reported in [27, 30]. It was found that these parameters have limited influence on the model dynamics as the relative displacements between the mass points in horizontal and diagonal directions are small.

IV. Experimental Work

In this section, a single TEPM is tested to show the benefits of introducing the tendon-driven mechanism to the pneumatic muscle actuator. The robot is then tested for stereotyped motions, such as elongation and bending, to validate the presented model. Finally, the characteristics of the robot system, such as hysteresis in bending motion, open-loop gain and tracking errors, are evaluated.

A. Test of a Single Actuator

The presented TEPM actuator can work in two modes as follows:

(1) The stepping motor is always disabled by applying a constant zero voltage signal at the ENA pin of the motor driver. In this mode the motor and the attached tendons will move passively, following the length change of the actuator caused by the pneumatic muscle. In other words, the actuator can be considered as a pure pneumatic muscle in this mode.

(2) If the error between the desired and the actual length of the TEPM is smaller than a given threshold, e.g. 3mm in our case, the stepping motor will be enabled by applying a 5V signal at the ENA pin of the motor driver to provide fine adjustment for the TEPM. Otherwise, the stepping motor will be disabled. In this mode, the attached tendon can be released or pulled by the motor and cooperate with the pneumatic muscle to drive the actuator, depending on the length error. Note that, the stepping motor will be turned on only if the length error is relative small. This is to avoid a large tension applied to the TEPM that may cause strong frictions at the actuator elements, such as the tendon block and the connector, or even buckling to the actuator.

The presented TEPM actuator is tested for linear movement in this section. The test bench is shown in Fig.5(a). Two tracking sensors are mounted at each end of the TEPM. The guider is used to prevent the actuator from bending since the muscle is compliant. The length of the actuator is obtained in

This article has been accepted for publication in a future issue of this journal, but has not been fully edited. Content may change prior to final publication. Citation information: DOI 10.1109/TMECH.2016.2636199, IEEE/ASME Transactions on Mechatronics

real time by calculating the distance difference between the two sensors.

A PID controller is used here to achieve the basic position control of the TEPM, as shown in Fig.5(b). The TEPM is controlled to reach three set points in sequence, 220mm, 230mm, and 240mm in length, from its initial length, 200mm. The tests were performed 3 times in mode 1 and mode 2, respectively. The results are given in Fig.6.

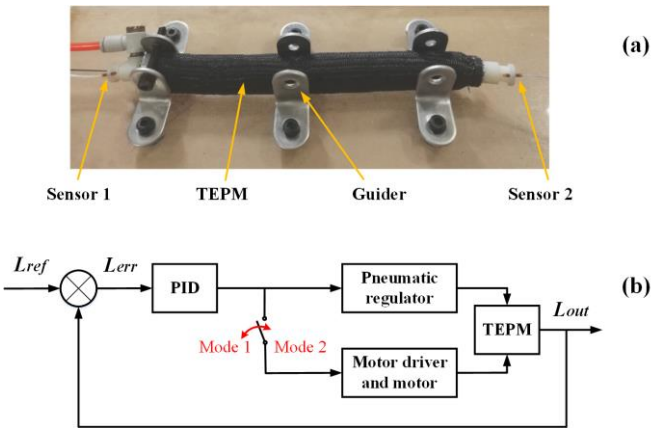

Fig. 5. Test of a single TEPM (a) test bench, (b) control scheme

It was found that, the average positioning error (AE) in mode 1 at set points 1, 2, and 3 are 1.85mm, 3.10mm, and 2.67mm, respectively. They are larger than those in mode 2, which are 0.81mm, 0.93mm, and 0.85mm, respectively. Moreover, the standard deviations (SD) of the three tests in mode 1 are 2.06mm, 3.36mm, and 3.51mm at the set points 1, 2, and 3, respectively, while they are 1.00mm, 0.87mm, and 0.98mm in mode 2.

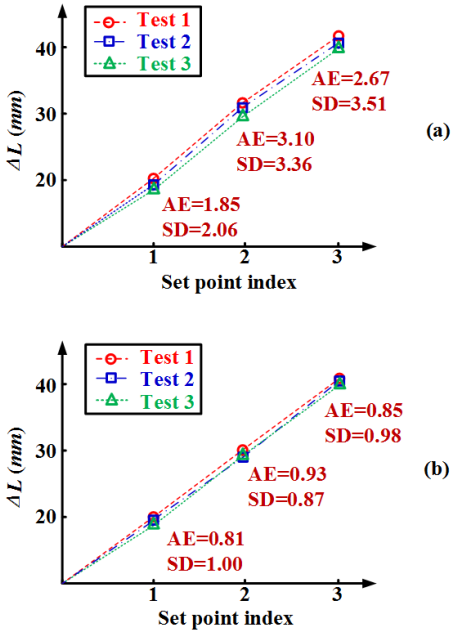

Fig. 6. Experimental results of set point control in (a) mode 1, (b) mode 2

The experimental results show that the average error and standard deviation produced in mode 1 are both larger than those in mode 2. Thus, the use of tendon control in a TEPM can improve the positioning accuracy and repeatability of the actuator. This is because the resolution of the pneumatic regulator is 0.5% of its full scale [34], while the resolution of the motor driver can achieve 0.015% of its full scale [35]. This means that the tendon control is more suitable for fine adjustment. Also, the tendon is less elastic than the air in the pneumatic muscle and therefore provides better repeatability than the pneumatic muscle alone.

Although the controller used in this section is primitive, it shows the benefits of using tendon control in addition to the pneumatic control. A more sophisticated controller would further improve the control performance of the TEPM, but controller development is outside of the scope of this paper and will be investigated in future.

B. Validation of the Dynamic Model

Elongation and bending motions are used to validate the model as they are the most common motion types for a continuum robot. The same inputs, including pressure and tension, are applied to the model and prototype, respectively. The resultant position of the model and the prototype are then compared.

The position of the robot body is defined by four reference points, s_i (i=1,2,3,4), where the sensors are mounted, Fig.2(a). The tracking system has been designed and fabricated to have high metal immunity [36], and the sensors are mounted in the plastic holders with an offset distance (40mm), from the backbone of the robot to further avoid distortion due to the metallic spring in the TEPM. Hence, the measurement of the robot backbone is proceeded as follows: (1) Positions of s_i are measured by the electromagnetic tracking system; (2) A Piecewise Cubic Hermite Interpolation (PCHIP) algorithm is used to generate the nominal backbone curve passing through s_i [37]. The purpose of using PCHIP is to provide a continuous backbone curve based on the discrete measure points. This helps to show the robot configuration intuitively, and can be used to estimate the errors at other points besides the measure points in future. The positional data of the robot is given in a global coordinate system G-xyz defined by the tracking device, whose origin G is at the center of the electromagnetic transmitter, the axis z is along the vertical direction, and the axis y is perpendicular to the plane formed by the actuators $A_{1,2}$ and $A_{1,3}$.

As there are four measured reference points along the robot length, the metrics to describe the modeling error could be the maximum error, average error, or root mean square error (RMSE), etc. In this paper, the RMSE is adopted according to

$$E=\sqrt{\frac{\sum_{i=1}^{4}[(x_{si}-x'_{si})^2+(y_{si}-y'_{si})^2+(z_{si}-z'_{si})^2]}{4}}=\sqrt{\frac{\sum_{i=1}^{4}\varepsilon_{si}^2}{4}} \quad (5)$$

where $[x_{si} \quad y_{si} \quad z_{si}]^T$ is the coordinates of the measured reference points s_i on the prototype, $[x'_{si} \quad y'_{si} \quad z'_{si}]^T$ is the coordinates of the corresponding reference points s'_i on the model, and ε_{ri} is the position difference between the points s_i and s'_i. Each motion was tested 3 times, and the results with middle level RMSE among the three tests shown as follows.

This article has been accepted for publication in a future issue of this journal, but has not been fully edited. Content may change prior to final publication. Citation information: DOI 10.1109/TMECH.2016.2636199, IEEE/ASME Transactions on Mechatronics

1) Elongation

Elongation is achieved by applying identical pressure to all TEPMs in any module as the pneumatic muscles used in the prototype are designed to extend when inflated. Figure 7(a) shows the configuration of the robot doing elongation, where the TEPMs in modules 1 and 2 are inflated with pressures of 0.2 MPa and 0.3MPa, respectively, while the tendons of all TEPMs are set to zero, Fig.7 (b). The reference points on the model and prototype are then identified and plotted in Fig.7 (c). It can be seen that the position error ε_{ri} at the reference points increases from 1.5mm to 7.4mm along the robot from the base to the tip as shown in Fig.7(d), and the RMSE of those points is 5.32mm (1.24% of the initial length of the robot) according to (5). The reason of the modeling error will be discussed at the end of this section.

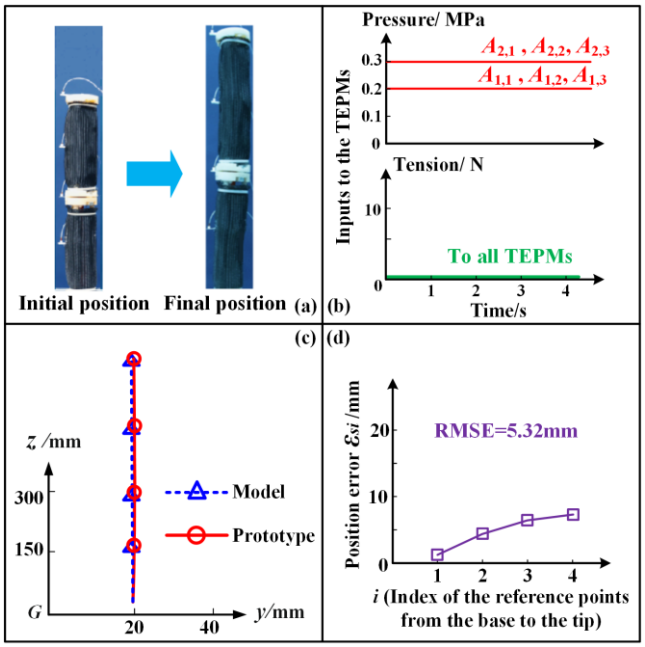

Fig. 7. Elongation of the robotic prototype

2) Double bends on the robot

Double bends is a combination of two singles bends on different modules. Figure 8(a) presents the bending motion simultaneously occurring on the modules 1 and 2. The corresponding inputs are shown in Fig.8(b), where the TEPMs $A_{2,1}$ and $A_{1,3}$ are inflated with a pressure of 0.25MPa while the tendons of TEPMs $A_{2,2}$ and $A_{2,3}$ are applied with a tension of 7N. The position error at the base reference point s_1 is 2.8mm, and increases to 11.3mm at the top reference point s_4. The RMSE at these points is 8.75mm (2.03% of the initial length of the robot), as shown in Fig.8 (c) and (d).

3) Dynamic bend

Figure 9(a) presents a whole arm bending motion from 0s to 3s. This is achieve by inflating TEPM $A_{1,1}$ and $A_{2,1}$ along one side of the modules 1 and 2 with a pressure of 0.15MPa. In the meantime, the tendons of TEPMs $A_{1,2}$, $A_{1,3}$, $A_{2,2}$ and $A_{2,3}$ on the opposite side of the modules are applied with a tension of 3N, Fig.9(b). To avoid oscillations during the movements the inputs are shaped to ramp signals from 0s to 3s. Figure 9(c) shows the position errors between the model and the prototype at the reference points over the time period from 0 to 3s. The maximum error of 20.1mm occurs at the reference point s_2 at time instant 2s.

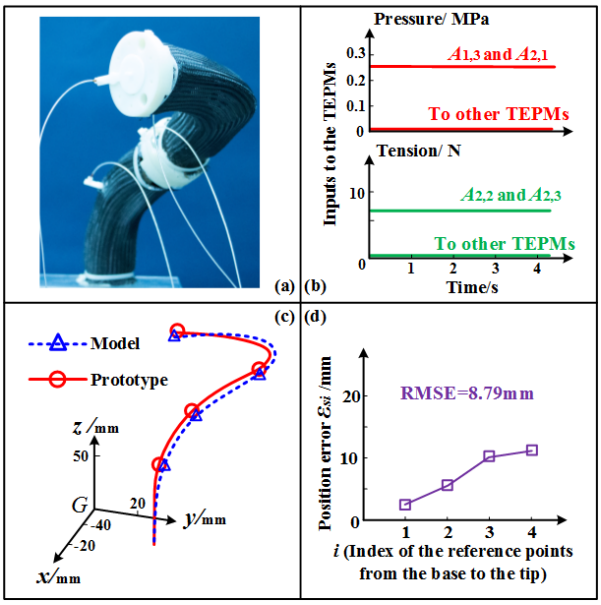

Fig. 8. Double bends occurring on two modules

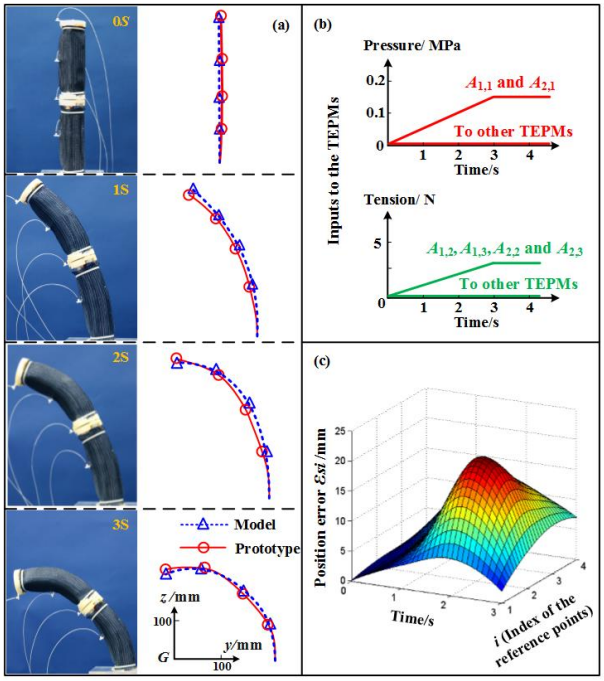

Fig. 9. Whole arm bending dynamics

4) Discussion of the modeling error

The modeling errors can be seen from Figures 7 to 9, where the static RMSE ranges from 5.3mm to 8.8mm (Figures 7 and 8), and the maximum dynamic error is over 20mm. The reasons for the errors are likely because the model error relies on the number of segments used in the model. Generally, the use of more segments will reduce the modeling error as it reduces the nonlinearity in each segment [30], and allows for smoother trajectory during bending motions. However, the modeling error cannot be reduced continuously once the number of segments reaches a specific number, e.g. $n_e = 6$ in our case. This

is because the modeling error mostly comes from other factors rather than the segment number at this stage.

The other factors introducing modeling errors can be that (1) the frictions among the TEPMs, connecting plates and sensor holders are not accounted for in the model; (2) the model is fully compliant yet the connecting plates and sensor holders in the robot are rigid; (3) the model ignores the uneven distribution of the mass in the real robot; (4) the parameters used in the model are not accurate enough. As the resulting error in the model is relatively small, these error can be evaluated in future, should more accurate results be required based on desired application.

C. Elastic Deformation and Resilient Motion of the Robot

To show the effect of structural deformation under external force the tip of the robotic prototype is subjected to an external force of 2.5N, normal to the robot backbone. The pneumatic pressure and tendon tension are set to zero in this case, which means the robot was passively deformed by the external force. Simulated and experimental results are compared in Fig. 10(a) where the RMSE between the model and the prototype is 8.60mm (2.0% of the initial length of the robot) and the bending angle is about 65°. Again, the errors are due to the rigid components and frictions in the prototype which are not considered in the model.

Due to the presence of the resilient spring in the TEPMs, the robot will return to straight position once the external force is canceled. This is different from the pneumatic continuum robots reported in [27, 30], which will remain curved even if the external force is canceled. Figure 10(b) shows the bending-return characteristics, hysteresis, of the presented robot and previous robot reported in [30], by gradually applying and canceling an external force to the robot tip. To compare them in the same scale, the external force and bending angle are normalized with respect to their maximum values. The results clearly show that the use of the resilient spring in the presented robot reduces the hysteresis from 33% to 7%, and eliminates the residual error when the external force returns to zero. Hence, the control accuracy of the presented robot is improved.

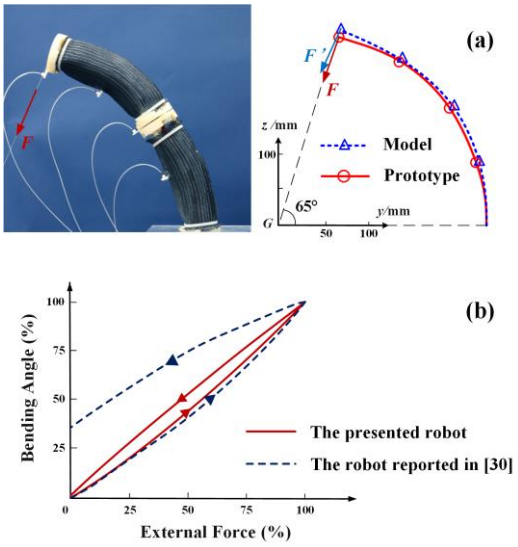

Fig. 10. (a) Bending deformation due to an external force, (b) Bending-return characteristics of the robot

D. Open-loop Gain of the Robotic System

In this paper, the open-loop gain is defined by the ratio of output change to the input change and used to analysis the influence of the TEPMs on the robotic system. For the presented robotic system, the inputs include the pneumatic pressure and the tendon tension while the output is considered as the robot position measured from the tip, i.e. the position of the reference point r_4. Since there are 6 TEPMs in the prototype, the total number of the inputs is 12. The position of the robot tip is defined by a column vector containing 3 elements, each of which represents the position component in x, y and z direction, respectively. Thus, the inputs and the outputs are related by

$$\boldsymbol{P} = \boldsymbol{G}\boldsymbol{u} \tag{6}$$

where $\boldsymbol{P}=[x_{s4}\ y_{s4}\ z_{s4}]^T$ is the position of the robot tip, $\boldsymbol{u}=[\boldsymbol{p}\ \boldsymbol{\lambda}]^T$ is the input vector in which $\boldsymbol{p}=[p_{1,1}\ p_{1,2}\ p_{1,3}\ p_{2,1}\ p_{2,2}\ p_{2,3}]^T$ and $\boldsymbol{\lambda}=[\lambda_{1,1}\ \lambda_{1,2}\ \lambda_{1,3}\ \lambda_{2,1}\ \lambda_{2,2}\ \lambda_{2,3}]^T$ are the pressure and tension of the TEPM actuator $A_{h,j}$ (h=1,2, j =1,2,3) respectively, and $\boldsymbol{G}$ is the open-loop gain matrix including 36 elements. As the presented robot is a nonlinear system, $\boldsymbol{G}$ will vary if the inputs or outputs change.

Although the comprehensive analysis of $\boldsymbol{G}$ is out of the scope of this paper, it is possible to take individual elements in the matrix $\boldsymbol{G}$ as examples to investigate the difference between the pneumatic control and tendon control. When the robot is moving, the position coordinates x_{s4}, y_{s4} may not change (e.g. elongation or bending within the y-z or x-z plane), but the position coordinate z_{s4} will always change. In other words, the elements in the third row of $\boldsymbol{G}$ will always have non-zero values. To make sure that we can observe non-zero elements in the experiment, two elements, $g_{3,3}$ and $g_{3,9}$ from the third row of $\boldsymbol{G}$, are selected here as examples to reflect the contributions of pressure and tension of the TEPM $A_{1,3}$ to the position coordinate z_{s4}.

In this experiment, the pneumatic actuation and the tendon actuation are enabled separately. First, the TEPM $A_{1,3}$ is pressurized with an input pressure $p_{1,3}$ to generate a bend on the module 1 while the tendons passively follow the movement. Then, the TEPM $A_{1,3}$ is deflated, and the stepping motor starts pulling its tendon with an input tension $\lambda_{1,3}$ to generate a bend again on the module. In either case, the position coordinate z_{s4} will decrease. To illustrate the input-output relations, the inputs, $p_{1,3}$ and $\lambda_{1,3}$, are expressed in a dimensionless manner by using percentage with respect to their maximum values. Figure 11(a) shows the position curve where the inputs are within an interval of 10% to 20%. The slopes of the curves indicate the values of $g_{3,3}$ and $g_{3,9}$, i.e. open-loop gains of the pressure control and tendon control, respectively.

Although the increase of the pressure and tension both result in a decrease of position coordinate z_{s4}, the slope of the pressure-position curve is greater than that of the tension-position curve. In other words, the absolute value of the open-loop gain of pressure control, $g_{3,3}$, is greater than that of tendon control, $g_{3,9}$. This is because the maximum force generated by the pneumatic muscle is larger than that generated by the stepping motor in the presented TEPM, meaning that the pressure control can achieve high strength and a wide range of position adjustment, while the tension control is suitable for

fine adjustment with relatively small strength. This is consistent with the aim of our design.

It is also found that, the standard deviation of the tip position, z_{s4}, due to the tension control of the tendon (1.33mm) is lower than that due to the pressure control of the pneumatic actuators (5.41mm). Thus, the tension control can generate motions with less oscillations, which is important to the system accuracy because the motor driver has higher resolution that the pneumatic regulators, as mentioned in Sec. IV (B). It is also important as the elasticity of the tendon is less than that of the air.

The experiment was repeated for the inputs within 45% to 55%, as shown in Fig.11(b), and similar results were found. The tension control allows for smaller open-loop gain and smoother motions.

In our design, the TEPM actuators are identical and evenly spaced 120° apart in a module. The two modules are identical as well. So it is reasonable to suppose that the qualitative conclusions obtained from one actuator in a module is applicable to the other actuators and module.

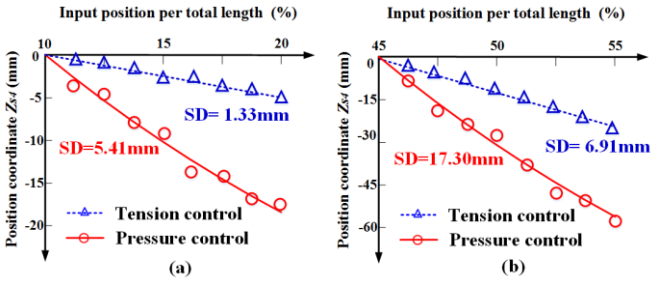

Fig. 11. Relationship between the inputs of the TEPM $A_{1,3}$ and the position coordinate z_{s4}

E. Position tracking

In this section, the robotic system is tested to evaluate its performance on position tracking. A desired circular trajectory of the robot tip, r_4, is given as

$$\begin{cases} x_d = 150cos\omega \\ y_d = 150sin\omega \\ z_d = 350 \end{cases} \quad (7)$$

where $\omega \in [0, 2\pi)$. As the robot consists of two serially connected modules, there are multiple possible configurations for the robot tip to reach a given position. To obtain a unique solution, an additional constraint that both modules have identical curvature during motion was applied to the model. The desired lengths of the TEPMs are then solved, and the TEPMs are controlled in modes 1 and 2, respectively, as described in Sec. IV (B).

The experiment was performed 3 times, and the average of these results are presented in Fig.12. It can be seen that the robot generally follows the desired trajectory when all actuators work in mode 1, Fig.12(a). However, the hybrid actuation in mode 2 achieves better performance, Fig.12(b), where the actual trajectory is closer to the desired one.

The detailed tracking errors in the x, y and z directions are plotted in Fig.12(c) and (d), and are characterized by a RMSE index with respect to 32 points on the trajectory ($0 \le \omega < 2\pi$). It was found that the hybrid actuation reduces the RMSE from 9.77mm in mode 1 to 5.60mm in mode 2. Errors are mainly due to the frictions in the robot that are not compensated for by the controller.

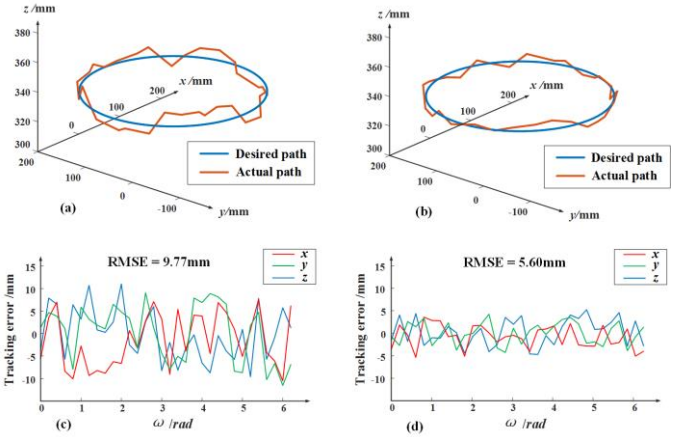

Fig. 12. Performance of position tracking (a) tracking path in mode 1, (b) tracking path in mode 2, (c) tracking errors in mode 1, (d) tracking errors in mode 2

V. CONCLUSIONS

This paper presents a novel continuum robot equipped with tendon embedded pneumatic muscle (TEPM) actuators. A pneumatic muscle with resilient spring to reduce hysteresis and residual error provides a majority of the driving force and working space, and a tendon is integrated along the length of the pneumatic muscle to enable fine adjustment of position.

A 3-D dynamic model based on a mass-damper-spring network is then validated to the robotic prototype and shows a good agreement between the two.

Compared with pneumatic muscle control alone, the tendon control provides higher accuracy, lower open-loop gain and reduces oscillations to the outputs, thus, the hybrid system provides the potential to improve the control performance of the robotic system. This design combines the advantages of pneumatic and tendon-driven actuation technologies in terms of compliance, strength and accuracy.

REFERENCES

[1] B. A. Jones and I. D. Walker, "Practical kinematics for real-time implementation of continuum robots", *IEEE Transactions on Robotics*, vol. 22, no.6, pp. 1087-1099. 2006.

[2] I. D. Walker, D. M. Dawson, T. Flash, F. W. Grasso, R. T. Hanlon, B. Hochner, W. M. Kier, C. C. Pagano, C. D. Rahn and Q. M. Zhang, "Continuum robot arms inspired by cephalopods", *Proceedings of the SPIE 5804* 303-14, 2005.

[3] H. Yuk, D. Kim, H. Lee, S. Jo and J. H. Shin, "Shape memory alloy-based small crawling robots inspired by C. elegans", *Bioinspiration & biomimetics*, vol.6, 046002, 2011.

[4] A. Menciassi, S. Gorini, G. Pernorio and P. Dario, "A SMA actuated artificial earthworm", *Proc. of IEEE International Conference on Robotics and Automation*, pp. 3282-3287, Hong Kong, China, 2004.

[5] H. R. Choi, K. Jung, S. Ryew, J. D. Nam, J. Jeon, J. C. Koo and K. Tanie, "Biomimetic soft actuator: design, modeling, control, and applications", *IEEE/ASME Transactions on Mechatronics*, vol.10, no.5, pp.581-593, 2005.

[6] D. B. Camarillo, C. F. Milne, C. R. Carlson, M. R. Zinn and J. K. Salisbury, "Mechanics modeling of tendon-driven continuum manipulators", *IEEE Transactions on Robotics*, vol.24, no.6, pp.1262-1273, 2008.

[7] C. Laschi, B. Mazzolai, V. Mattoli, M. Cianchetti and P. Dario, "Design of a biomimetic robotic octopus arm", *Bioinspiration & biomimetics*, vol.4, 015006, 2009.
[8] Q. Peng, C. Qiu, H. B. Liu, J. S. Dai, L. Seneviratne and K. Althoefer, "A novel continuum manipulator design using serially connected double-layer planar springs", *IEEE/ASME Transactions on Mechatronics*, doi 10.1109/TMECH.2015.2498738, 2015.
[9] K. Zhang, C. Qiu and J. S. Dai, "An extensible continuum robot with integrated origami parallel modules", *ASME Journal of Mechanisms and Robotics*, doi:10.1115/1.4031808, 2015.
[10] C. P., Chou and B. Hannaford, "Measurement and modeling of McKibben pneumatic artificial muscles", *IEEE Transactions on Robotics and Automation*, vol.12, no.1, pp. 90-102, 1996.
[11] D. Rus and M. T. Tolley, "Design, fabrication and control of soft robots", *Nature*, vol.521, pp.467-475, 2015.
[12] G. Immega and K. Antonelli, "The KSI tentacle manipulator", *Proc. of IEEE International Conference on Robotics and Automation*, pp. 3149-3154, Nagoya, Japan, 1995.
[13] W. McMahan, B. A. Jones and I. D. Walker, "Design and implementation of a multi-section continuum robot: air-Octor", *Proc. of IEEE/RSJ International Conference on Intelligent Robots and Systems*, pp. 2578-2585, Alberta, Canada , 2005.
[14] C. Laschi, M. Cianchetti, B. Mazzolai, L. Margheri, M. Follador and P. Dario, "Soft robot arm inspired by the octopus", *Advanced Robotics*, vol.26, no.7, pp. 709-727, 2012.
[15] A. Shiva, A. Stilli, Y. Noh, A. Faragasso, I.D. Falco, G. Gerboni, M. Cianchetti, A.Menciassi, K. Althoefer, H.A. Wurdemann, "Tendon-based stiffening for apneumatically actuated soft manipulator", *IEEE Robotics and Automation Letters*, 1, pp.632–637, 2016.
[16] M. Ciancetti, T. Ranzani, G. Gerboni, I. De Falco, C. Laschi, and A, Menciassi, "STIFF-FLOP Surgical Manipulator: Mechanical Design and Experimental Characterization of the Single Module", *Proc. IEEE/RSJ International Conference on Intelligent Robots and Systems*, pp. 3576-3581, Tokyo, Japan, 2013.
[17] B. Conrad and M. Zinn, "Closed Loop Task Space Control of an Interleaved Continuum-Rigid Manipulator", *Proc. IEEE International Conference on Robotics and Automation*, pp. 1743-1750, Seattle, WA, 2015.
[18] M. W. Hannan and I. D. Walker, "Kinematics and the implementation of an elephant's trunk manipulator and other continuum style robots", *Journal of Robotic Systems*, vol.20, no.2, pp. 45-63, 2003.
[19] I. S. Godage, E. Guglielmino, D. T. Branson, G. A. Medrano-Cerda and D. G. Caldwell, , "Novel modal approach for kinematics of multisection continuum arms", *Proc. of IEEE/RSJ International Conference on Intelligent Robots and Systems*, pp. 1093-1098, San Francisco, USA, 2011.
[20] R. J. Webster and B. A. Jones, "Design and kinematic modeling of constant curvature continuum robots: a review", *The International Journal of Robotics Research*, vol.29, no.13, pp. 1661-1683, 2010.
[21] E. Tatlicioglu, I. D. Walker and D. M. Dawson, "Dynamic modelling for planar extensible continuum robot manipulators", *Proc. of IEEE International Conference on Robotics and Automation*, pp. 1357-1362, Roma, Italy, 2007.
[22] E. Tatlicioglu, I. D. Walker and D. M. Dawson, "New dynamic models for planar extensible continuum robot manipulators", Proc. of IEEE/RSJ International Conference on Intelligent Robots and Systems, pp. 1485-1490, San Diego, U.S., 2007.
[23] B. A. Jones, R. L. Gray and K. Turlapati, "Three dimensional statics for continuum robotics", *Proc. of IEEE/RSJ International Conference on Intelligent Robots and Systems*, pp. 2659-2664, St. Louis, U.S., 2009.
[24] N. Giri and I. D. Walker, "Three module lumped element model of a continuum arm section", *Proc. of IEEE/RSJ International Conference on Intelligent Robots and Systems*, pp. 4060-4065, San Francisco, U.S., 2011.
[25] Y. Yekutieli, R. Sagiv-Zohar, R. Aharonov, Y. Engel, B. Hochner and T. Flash, "Dynamic model of the octopus arm. I. Biomechanics of the octopus reaching movement", *Journal of Neurophysiology*, vol.94, no.2, pp.1443-1458, 2005.
[26] C. Qiu, K. Zhang and J. S. Dai, "Repelling-screw based force analysis of origami mechanisms", *ASME Journal of Mechanisms and Robotics*, doi:10.1115/1.4031458, 2015.
[27] R. Kang, D. Branson, T. Zheng, E. Guglielmino D. G. Caldwell, "Design, modeling and control of a pneumatically actuated manipulator inspired by biological continuum structures", *Bioinspiration & biomimetics*, vol.8, no.3, 036008, 2013.
[28] J. Mather, "How do octopuses use their arms", *Journal of Comparative Psychology*, vol.112, no.3, 306-316, 1998.
[29] D. Trivedi, C. D. Rahn, W. M. Kier and I. D. Walker, "Soft robotics: biological inspiration, state of the art, and future research", *Applied Bionics and Biomechanics*, vol.5, no.3, pp.99-117, 2008.
[30] Y. Guo, R. Kang, L. Chen, J.S. Dai, "Dynamic modeling for a Continuum Robot with Compliant Structure", *Proc. of the ASME 2015 International Design Engineering Technical Conferences & Computers and Information in Engineering Conference IDETC/CIE*, 46683, Boston, U.S., 2015.
[31] W. S. Rone and P. Ben-Tzvi, "Continuum robot dynamics utilizing the principle of virtual power", *IEEE Transactions on Robotics*, vol. 30, no. 1, pp. 275-287, 2014.
[32] D. Caldwell, G. Medrano-Cerda and M. Goodwin, "Control of pneumatic muscle actuators", *IEEE Control Systems Magazine*, vol.15, pp.40-48, 1995.
[33] C. Chou and B. Hannaford "Measurement and modeling of McKibben pneumatic artificial muscles", *IEEE Transactions on Robotics and Automation*, vol.12, no.1, pp.90-102, 1996.
[34] Manual of the SMC ITV pneumatic regulator, http://www.smc.com.cn/
[35] Datasheet of the M415B motor driver, http://www.docin.com/p-130124-5868.html
[36] Ascension 3D Guidance, http://www.ascension-tech.com/products/trakstar-drivebay/
[37] PCHIP algorithm, www.mathworks.com/help/matlab/ref/pchip.html

Rongjie Kang received his undergraduate and master's degrees in automation science, and Ph.D in mechanical engineering from the Beihang University, China. He is currently an associate professor in the school of mechanical engineering, Tianjin University, China. His research interests include continuum robots, bio-inspired robots, fluid power control, and mechatronic systems.

Yong Guo received his undergraduate's degree in industry design and master's degree in mechanical engineering from Tianjin University, China. His research interests include soft robots and robotic dynamics.

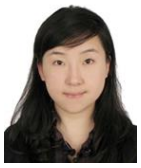

Lisha Chen received her undergraduate and master's degrees in automation science from the Beihang University, China, and Ph.D. from the University of Genova, Italy. She is currently a lecturer in the School of Mechanical Engineering, Tianjin Polytechnic University, China. Her research interests include mechanisms and robotics, variable stiffness actuators and control theory.

David T. Branson III received his undergraduate and master's degrees in mechanical engineering from the University of Wisconsin-Madison, USA, and Ph.D. from the University of Bath, UK. He is currently an Assistant Professor in the Faculty of Engineering – University of Nottingham, UK. His research interests are in the areas of modelling and control of non-linear systems undergoing large deformations/displacements with application to the design and control of robotic systems for manufacturing and healthcare purposes; wearable monitoring systems; and controlled continuum arms/surfaces.

Jian S. Dai received his undergraduate and master's degrees in mechanical engineering from the Shanghai Jiaotong University, China, and Ph.D. from the University of Salford, UK. He is a fellow of ASME, fellow of IMechE and chair professor of Mechanisms and Robotics at Centre for Robotics Research, King's College London, University of London. He has been working in the field of mechanisms and robotics in the past 25 years and published over 400 peer-reviewed papers (more than 200 on ISI journals). His research is on theoretical and computational kinematics, reconfigurable mechanisms, dexterous mechanisms and manipulators, end-effectors and multifingered hands. He won the Mechanisms and Robotics Award given annually by the Mechanisms and

Robotics Committee of the American Society of Mechanical Engineers (ASME), to engineers known for a Lifelong Contribution to the field of mechanism design or theory. He was recipient of several journal and conference best paper awards and has been taking Associated Editor of IEEE Transactions on Robotics, ASME Transactions: Journal of Mechanisms and Robotics, Mechanism and Machine Theory, and Robotica.